PCCP

Accepted Manuscript

ROYAL SOCIETY OF CHEMISTRY

www.rsc.org/pccp

Journal Name

ARTICLE TYPE

Cite this: DOI: 10.1039/xxxxxxxxxx

Polarized emission from stretched PPV films viewed at the molecular level†

Rodrigo Ramos,[a] Melissa F. Siqueira,[b] Thiago Cazati,[b] Roberto M. Faria,[c] and Marilia J. Caldas [a]

Received Date
Accepted Date

DOI: 10.1039/xxxxxxxxxx

www.rsc.org/journalname

We present a study on the photoluminescence (PL) of thin films of poly-(p-phenylene vinylene) (PPV), non stretched and uniaxially stretched. The experimental study was carried out using linear polarized light as the excitation beam, either oriented parallel or perpendicular to the stretch axis (***S***). The results showed that when the excitation light source has polarization perpendicularly oriented to the stretch direction, the emitted PL presents maximum intensity in the orientation ***S***, and a minimum in the direction orthogonal to ***S***. In order to understand this interesting phenomenon we employ theoretical simulations at the atomistic level. We use classical molecular dynamics to simulate amorphous PPV films, non-stretched and stretched, from which we find a tendency of overall alignment of PV units to ***S***, and of local clustering in herring-bone and π-stacking partial symmetries. Our study of optical activity of this kind of clusters, performed through quantum semi-empirical method, allows us to explain this polarization conversion behavior, and indicates the possibility of using underivatized PPV as the active layer for polarized electroluminescent devices.

1 Introduction

The conjugated polymer poly-*p*-phenylene-vinylene (PPV) has been intensively studied[1–4] due to its potential for applications in the field of organic electronics, in particular for optoelectronic devices. PPV belongs to a class of luminescent materials[5,6] whose optical emission properties can be designed by tailoring the internal morphology of the polymer film in the active layer.[7–9] Ideal linear conjugated polymers by construction absorb and emit light with well-defined polarization along the chain backbone axis, however, when dispersed in a solvent or condensed as a film (usually in disordered morphology) the chain backbone orientation is homogeneously distributed in all directions, and this polarization characteristic is lost. Exploring anisotropic features and local ordering effects opens the possibility for engineering physical properties, and conjugated polymer films with a reasonable degree of alignment are promising materials for polarized electroluminescent devices.[8,10–12]

In thin polymeric PPV films crystalline grains or domains are randomly dispersed in an amorphous phase, as seen from infrared and crystallographic analysis.[2,3] Morphological anisotropy can be achieved[2,7] but it is not known if always by overall alignment of crystallites, or also by simple alignment of polymer chains in the formerly isotropic distribution of the amorphous domains, with no crystalline arrangement. There are different routes for obtaining chain orientation and/or crystallinity, usually associated with stretching of the film either during the process of polymerization from precursor, or after polymerization; other processes such as rubbing are also becoming feasible.[13] Increase of charge carrier mobility in conjugated polymer films brought by molecular orientation is already a well known phenomenon,[4,6,14–17] which has been associated with increasing

[a] *Instituto de Física, Universidade de São Paulo, Rua do Matão s/n, trav. R 187, 05508-900, São Paulo-SP, Brazil. E-mail: rramos@if.usp.br*
[b] *Departamento de Física, Universidade Federal de Ouro Preto, 35400-000, Ouro Preto-MG.*
[b] *Instituto de Física de São Carlos, Universidade de São Paulo, 13560-970, São Carlos-SP*

planarity of the polymer backbones, and consequent increase of conjugation length. After stretching, the degree of orientation can also be probed through pressure-induced effects on optical properties,[18,19] that highlight the relevance of inter-chain packing morphologies in addition to intra-chain ordering and backbone alignment.

Indeed, an interesting effect of polarization of absorption/emission has been detected[9] where, for highly oriented PPV samples, incident light polarized perpendicular to the stretch direction converts in emission polarized parallel to the stretch direction. We here investigate this effect by complementary experimental/theoretical studies of stretched PPV films. We carried out UV-Vis measurements using polarized incident light, parallel or normal to the stretch axis, and analysing the polarization of the emitted light we find the same aforementioned conversion properties. We also performed theoretical simulations to study the effect of stretching on PPV films, using Classical Molecular Dynamics for the structural properties and the well-established ZINDO/S method[20] for the optical properties. Our results strongly suggest that the conversion of polarization, perpendicular to parallel to the draw direction, is originated in the amorphous domains. In section 2 we describe our experimental procedure and results, in section 3 we describe the theoretical simulation methodology; we then describe and discuss our results in section 4.

2 Experimental Results

We obtained PPV from its precursor, the poly(xylylidene tetrahydrothiophenium chloride) (PTHT), which was synthesized following the standard chemical route.[2] PTHT films 500 nm thick were deposited on a Teflon-tape (250 μm thick) by spin-coating a mixed aqueous solution of PTHT with dodecylbenzene sulfonic acid (DBSA) at 1.6:2 wt/wt. PTHT was then converted to PPV by an efficient thermal treatment technique.[21,22] PPV-Teflon bilayers were uniaxially stretched, which allowed us to obtain films with stretch ratio up to $\lambda = 4$. The stretch ratio λ is here defined as $\lambda = (l/l_0)$, being l the length of the uniaxially stretched sample and l_0 its initial length. Polarized photoluminescence (PL) experiments were carried out to analyze the optical anisotropy of the stretched PPV thin layers, by making use of a He-Cd laser (442 nm, 25mW/cm^2) as excitation source. To perform measurements of the intensity of PL emitted light according to its polarization, an analyzer was placed between the sample and the detector. The whole procedure –stretching, illumination and emission analysis– was undertaken under vacuum so as to avoid photo-oxidation of the sample. The experimental setup of polarized photoluminescence and optical absorption experiments are similar to that used in experiments carried out in oriented Langmuir-Blodgett films from a PPV derivative.[23] Here, we take the excitation wavelength (442 nm) at the maximum of the optical absorption spectra there recorded, while the emission was collected at the region of the maximum fluorescence intensity ($\sim$ 520 nm).[22,23]

Our experiments of optical absorption showed that the absorption intensity of a non-stretched film is the same irrespective of the orientation of the polarization of the incident light. On the other hand, the response of the optical absorption changed with the orientation of the polarization of light for stretched samples: the closer (more distant) was the orientation of polarization of light relative to the stretch direction, the higher (lower) was the intensity of the optical absorption, as expected. Afterwards, we carried out experiments of PL emitted light with non stretched and stretched samples. In such measurements two orientations for the linear polarization of the incident beam were used: parallel to the direction of the stretch ($I_{//}$), and perpendicular to it ($I_{\perp}$). For a non stretched sample ($\lambda = 1$), the PL intensity exhibited maximum values (peaks) when the orientation of the analyzer was aligned with the polarization of the incident light, $I_{//}$ or $I_{\perp}$, *i.e.* when the angles between them were 0°, 180° and 360°. In this case, PL showed minimum values (valleys) when these angles were 90° and 270°. Figure 1(a) depicts experimental results, in which the analyzer was rotated from 0° to 360°, for incident laser beam parallel ($I_{//}$) or perpendicular ($I_{\perp}$) to the direction of the stretch axis ($\boldsymbol{S}$). In summary, we find the expected results for optical absorption and emission.

The interesting result was observed when similar experiments were repeated with stretched samples. Figure 1(b) shows the PL intensity of the emitted light for a sample with stretch ratio $\lambda = 4$. For parallel incident beam ($I_{//}$) the PL peaks were recorded at 0°, 180° and 360°, as expected. However, when the incident beam was polarized perpendicular to the stretch direction ($I_{\perp}$), the emission peaks were recorded also close to 0°, 180° and 360°, showing a shift of approximately 90° in comparison with results obtained for non stretched samples, *i.e.* where we had valleys, peaks were now registered. In addition, we also observed that as the film was stretched from $\lambda = 1$ to $\lambda = 4$, the peaks and valleys shifted gradually to the maximum δ of 90°. This conversion of polarization cannot be explained only by crystallites reorientation, and motivated our complementary theoretical study.

3 Theoretical Simulations

The anisotropy of the optical properties coming from the stretching of the film described above could be in the first place associated to the characteristics of the crystallites in the film, that is, orientation with respect to the draw direction of the crystallite $\vec{c}$ axis (coincident with the backbone axis of the chains). However, underivatized PPV is known to crystallize in herring-bone (HB) symmetry. Now, it is also known, from theoretical studies of the optical properties of crystalline HB PPV,[24–26] that absorption in the $I_{\perp}$ configuration is extremely weak, and furthermore the lowest optical peak is dark, that is, light absorbed in any polarization direction decays to the optically inactive state. As such,

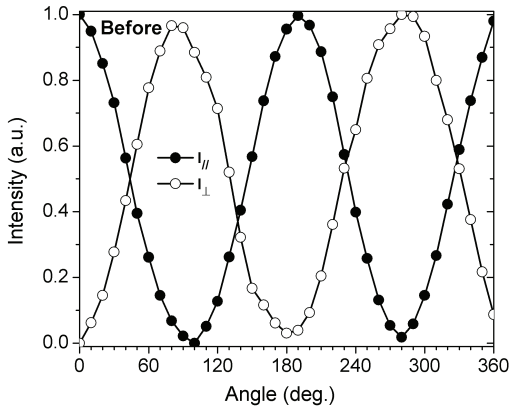

(a)

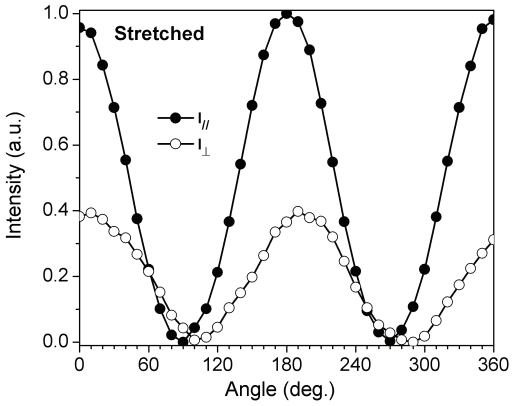

(b)

Fig. 1 Integrated photoluminescence spectra of PPV films (a) before $\lambda = 1$ and (b) after $\lambda = 4$ stretching. The angle in the abscissa defines the direction of the emitted light relative to the stretch direction. Solid circles refers to light emitted when the incident light is polarized parallel ($I_{//}$) to the stretch direction, open circles incident light polarized perpendicular ($I_{\perp}$) to the stretch direction.

once the crystallites are aligned not only absorption decreases but also emission is severely quenched in any direction. On the other hand, stretching can have also a strong effect on the amorphous regions, and thus we here investigate, by different methodologies in an atomistic picture, the impact of stretching on amorphous films of PPV, and the possible effect on the optical properties. We use for that Classical Molecular Dynamics, from where we extract the behavior of the organic material with draw ratio, regarding intra-chain characteristics (linearity, alignment with the draw vector) and inter-chain packing (local alignment and ordering of neighbor chain segments). We next study the effect of local packing on the optical properties through quantum semi-empirical calculations for different oligomer clusters.

3.1 Amorphous PPV Films, Isotropic and Stretched

As highlighted above, we need for this study a sound description of morphological characteristics of a polymer film in the amorphous configuration. It has already been noted in the literature that this task is best carried out through Molecular Dynamics (MD) simulations[27] however, for the minimum size of the system we need, in terms of number and length of polymer chains, the task cannot yet be performed through *ab initio* methods. We thus use a classical modeling (CMD) well-adapted for the specific system here, capable of description of the basic Carbon-Carbon and Carbon-Hydrogen bonds and interactions. We need description not only of intra-chain geometrical properties (bond lengths, bond angles) but also, and very important, of inter-chain properties that depend on non-bonded interactions.

For the bonded interactions we use the well-known Universal Force Field (UFF),[28] which however fails to give elastic characteristics of PPV films with the desired accuracy. The non-bonded interactions, Coulomb and van der Waals (vdW), were then adjusted[29] based on *ab initio* density functional theory studies of several model PV systems. In this case, it was adopted the evaluation of vdW interactions[30] as implemented in the AIMS package,[31] which is consistent from start with the concept of Hirshfeld partial charges[32] that was used for the Coulomb potentials. It was found one can adopt the same (fixed) charges and vdW parameters for C-atoms bonded to two C- and one H-atom, independently of the mer (phenylene or vinylene), while C-atoms bonded only to C-atoms need Q=0 and a different vdW parameter. In our approach thus the bonded energies remain the same as those defined in the standard UFF, however the non-bonded energies require to define for the resonant C-atoms two different types, which were named $C_{R\alpha}$ (non-charged) and $C_{R\beta}$ (charged), while the vinylene C-atom was named plain C_{β} (charged); the non-bonded parameters for the H-atom were also recalculated*. This procedure proved to give excellent approximations for the elastic coefficients for a wide range of systems.[29] We name our implementation *n*UFF.

The PPV amorphous films simulated here are built from reasonably long chains P26V25 containing 25 monomeric units (PV) and a phenylene cap, and each simulation cell of the (periodic) infinite film contains 40 chains with a total of 14480 atoms per cell. Initial samples were constructed by disposing randomly 40 linear chains in four layers; in order to avoid molecular super-

* For the Lennard-Jones $V_{LJ} = \varepsilon[(r_0/r)^{12} - (r_0/r)^6]$, with ε in kcal/mol and r_0 in Å and with charges in electron units e, we find $\varepsilon = 0.069800, r_0 = 3.850$ and Q=0 for $C_{R\alpha}$; $\varepsilon = 0.051478, r_0 = 3.975$ and Q= -0.05 for $C_{R\beta}$ and C_{β}; $\varepsilon = 0.029500, r_0 = 2.830$ and Q=+0.05 for H.

positions these initial models were built with large spacing between chains resulting in initial densities lower than 0.2 g/cm^3. First we performed systematic homogeneous reductions of cell parameters, intercalated with molecular mechanics (MM) optimizations and NVT dynamics, at T=300K; the minimum of total vdW energy of the cell is used to find the optimal region of cell volume, and a final NPT cycle is performed: this procedure avoids spurious too-high temperature steps. Typical converged densities for amorphous models are around 0.9 – 1.0 g/cm^3, and the final (supercell and atomic) temperature was fluctuating less than 1% around the temperature of the thermal reservoir. To simulate stretching we adopted a similar procedure, starting from the relaxed cell, then proceeding with step-by-step elongation of one cell axis with natural adjustment of the other two by MM+NVT cycles. Figure 2(a) shows snapshots of our model film taken for the non-stretched situation and for 50% of stretching (λ=1.5).

We followed the variation of polymer morphology caused by the stretching procedure through statistical analysis of the chain distributions in the film, considering the local environment of each mer. We recall that crystalline packing of PPV chains can assume HB symmetry, usual for non-functionalized PPV, or else π-stacking symmetry (π-S) in this case more often for derivatized polymers such as MEH-PPV[33]. As shown in Figure 3(b) and (c), phenylene and vinylene units face each other in the π-S arrangement, while in the HB conformation there are 2 PV segments (from two neighbor chains) in the unit cell, also with a similar phenylene-vinylene displacement but with a setting angle[3] of around 56-68°. These characteristics will be analysed for the amorphous regions as described in the next section.

For the optical signatures we have chosen finite oligomer clusters, compatible with the broken symmetry of an amorphous environment, with *partial* HB and π-S local conformations. The semi-empirical ZINDO/S method used here,[20] including single-excitations configuration interaction (CIS), has been shown to furnish sound results for π-conjugated stacked systems.[34–36] These calculations were carried out via the Cerius 4.6 package,[37] including 30 occupied to 30 unoccupied states for the single excitations.

3.2 Morphology Analysis

We performed two distinct analysis of the films, focusing on intra- and inter-chain arrangement. Starting with the intra-chain morphology, we evaluated the degree of linearity using the radius-of-gyration, R_g. For the inter-chain properties we employed two correlation functions calculated between phenylene and vinylene units within a cutoff radius of 5Å, equations 1 and 2, which are computed over the thermal sampling. $A(i,j)$ evaluates the axial alignment, so we can identify parallel segments, and $E(i,j)$ clarifies the relative orientation:

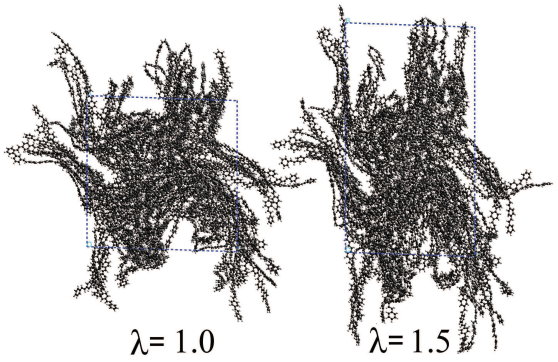

Fig. 2 Snapshots taken from CMD simulations for the non stretched film (left) and for a stretching ratio of $\lambda = 1.5$ (right).

$$A(i,j) = |\hat{\mathbf{a}}_i \cdot \hat{\mathbf{a}}_j| \quad (1)$$

$$E(i,j) = (|\hat{\mathbf{n}}_i \cdot \hat{\mathbf{r}}_{ij}| + 1)(|\hat{\mathbf{n}}_j \cdot \hat{\mathbf{r}}_{ij}| + 1)/4, \quad (2)$$

where the *"i"* (*"j"*) indexes refer to phenylene (vinylene) units, represented in Figure 3. The versors **a** define the axis of each unit (phenylene or vinylene), and **n** the normal to each unit plane, while $\mathbf{r}_{ij}$ are the versors between phenylene/vinylene units, as also represented in Figure 3. The factor 4 in eq. 2 is inserted to normalize $E(i,j)$ in the ideal (crystalline) π-stacking to 1.

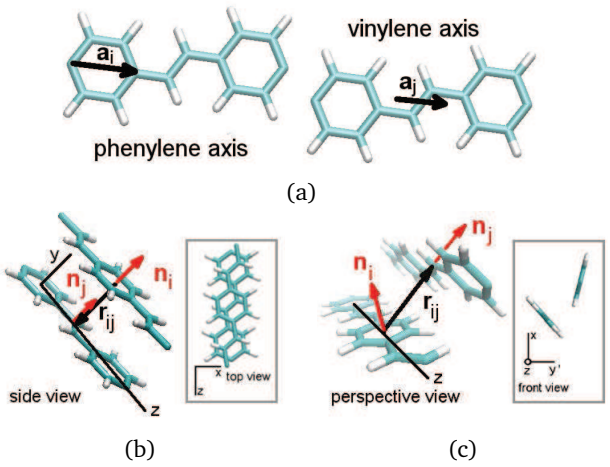

Fig. 3 Unit vectors used to identify the alignment and packing: (a) Representation of $\mathbf{a}_i$ phenylene axis, $\mathbf{a}_j$ vinylene axis. To vinylene $\mathbf{a}_j$ axis is defined by the average of $C_{R\alpha} - C_\beta$ bonds. (b, c) Local arrangements of chain segments in a condensed situation: π-S (b) and HB (c). $\mathbf{r}_{ij}$ vector joining phenylene and vinylene units, $\mathbf{n}_i$ and $\mathbf{n}_j$ normal axis to the phenylene or vinylene planes.

In both π-S and HB arrangements the axis of neighbor chains

are parallel, and hence such structures have $A(i,j) = 1$. $E(i,j)$ as defined above is in the range from 0.25 to 1, and can be used to find the local structures π-S and HB. For structures close to π-S we have $E \approx 1$, with the phenylene-vinylene distance $r_{ij} \approx 4.7$Å, and close to HB the range is $0.61 \leq E \leq 0.86$, with $r_{ij} \approx 5.4$Å. Finally, the alignment of the chains along the stretch direction is also analysed , by calculating the projection of each PV unit $\mathbf{R}_i$ (Figure 4) along the stretch direction $\boldsymbol{S}$ by the scalar product $\mathbf{R}_i \cdot \boldsymbol{S}$.

4 Simulation Results

We show in Figure 4(a) two typical, different behaviors for individual chains during the stretch procedure: on the left we show a chain that assumes overall a more linear character, elongates acquiring a larger R_g, and on the right another chain that folds (smaller R_g), due to inter-chain local arrangements or "knots". As can be seen in Figure 4(b), an initial concentrated pattern of R_g values between 30 and 35Å spreads with stretching over a wider range of values, giving place to a bimodal pattern as the stretching increases. That is, the evolution of the R_g values clearly showed two groups: one set of oligomers that extend, and another that fold, with presence mostly of kinks (not trans-cis transitions) as also illustrated in the same Figure 4. On the other hand, if we measure the overall alignment of mers along the stretch direction, Figure 4(c), we see a clear tendency to follow the draw, that is, we will find more segments aligned with the stretch direction even for the folded chains.

The number of kinks in a chain can be calculated by the distribution of vinylene–dihedral angles. The kink is characterized by dihedral values around 90°, while values close to 180° (0°) can be attributed to local linear trans (cis) segments. In Figure 4(d) we present the dihedral distributions for (left) elongated and (right) folded polymers, where we can see that the kink ratio related to the elongated subset is reduced after 100% stretch (10% to 4%), and increases for the set that undergoes folding (15% to 18%).

To evaluate the inter-chain packing, we show in Figure 5 the simultaneous correlation of the functions $E(i,j)$ and $A(i,j)$ defined above, for a collection of 100 samples along the CMD simulations. Starting with the analysis of the non stretched film, we see a natural inter-chain alignment of local character, coming from the conjugated nature of the polymer (not along any particular external direction). After stretching we see a definite increase of local inter-chain alignment. However, we also see that we cannot clearly distinguish a preferential inter-chain orientation, π-S or HB.

Therefore the most significant morphological signatures induced by the uniaxial stretch were observed to be i) a high enhancement of segments aligned parallel to the stretch direction, and ii) relevant increase in the number of local inter-chain parallel alignments.

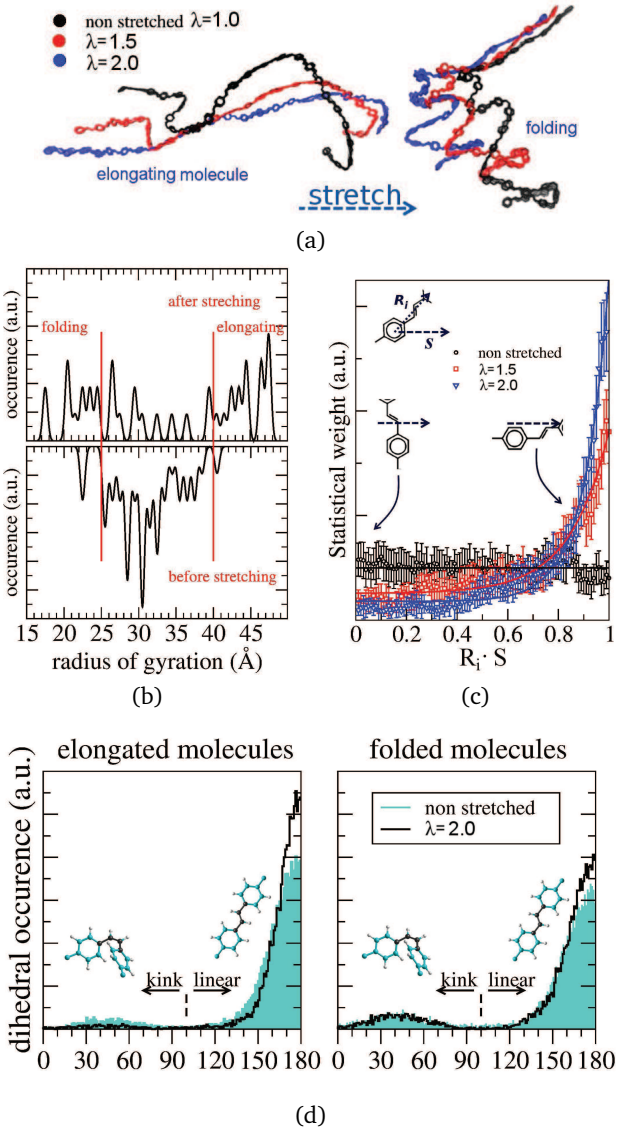

Fig. 4 Evolution of morphological properties with stretching: (a) examples of different trends for different oligomers, elongating (left) and folding (right); (b) distribution of R_g values from non stretched (lower panel) to $\lambda = 2$ stretched configuration (upper panel) (gaussian broadening of 0.1Å); (c) chain alignment to stretching direction, non stretched ($\lambda = 1$), stretched $\lambda = 1.5$, and $\lambda = 2.0$ (error bars are obtained through standard deviation over the sampling of configurations); (d) intramolecular dihedral distribution function, vinylene dihedrals, for the elongated (left) set of oligomers compared to the folded set (right).

4.1 Optical properties

We now address the effect of morphology on the optical properties of an amorphous film, working on simple models built from the signatures found in this work. From previous theoretical studies there is sufficient evidence that the symmetries of crys-

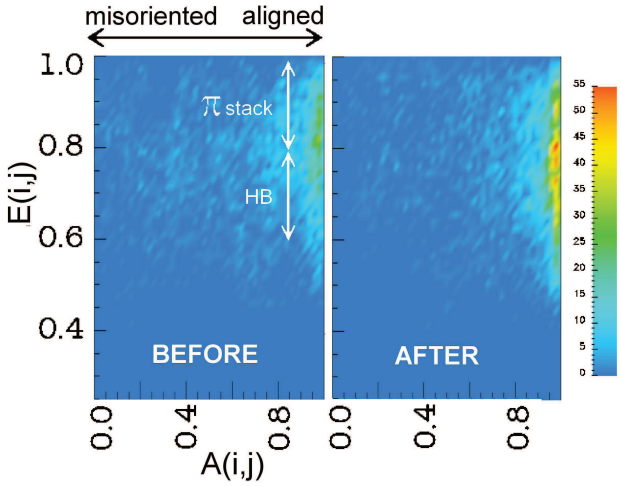

Fig. 5 Color maps for the identification of local HB and π-S distributions for the film. The figures are histograms of $E(i,j) \times A(i,j)$ calculated for every *i,j* (phenylene-vinylene) pair, inside 5Å cutoff, for the (a) non-stretched $\lambda = 1$ and (b) stretched $\lambda = 2$ film. The maps are built from 25 snapshots in intervals of 0.1ps (time step = 1fs) after NVT equilibration, in both cases.

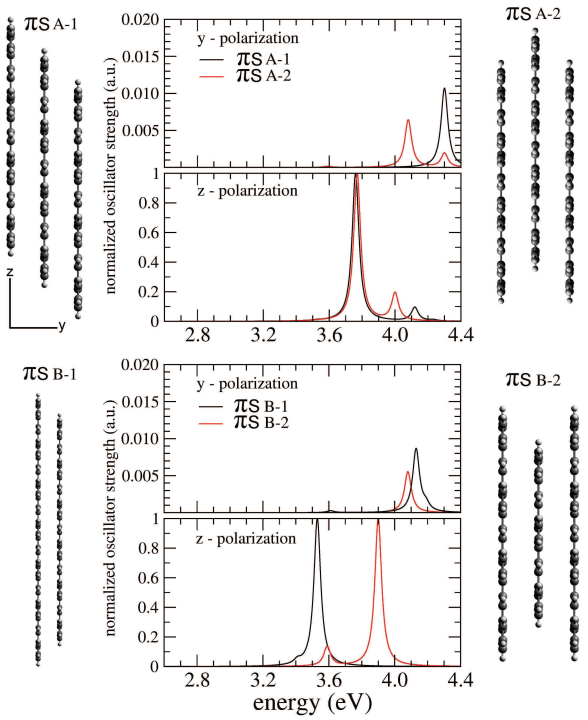

Fig. 6 Electronic absorption spectra calculated for different oligomer clusters in partial π-stacked local arrangements, as sketched on the left and on the right: πS A-1 and πS A-2 with P4V3 oligomers, πS B-1 with P7V6 and P6V5, and πS B-2 with P4V3 and P3V2. In each case, at the top the contribution of polarization intensity along the y-axis (perpendicular to the chain backbone), bottom along the z-axis (parallel). The spectra are obtained through a Lorentzian broadening of 25 meV, and further normalized in each calculation by setting to 1.0 the main peak in the chain direction.

talline packing have a direct effect on absorption and emission intensities, and in particular that the conversion of perpendicular polarized absorption to parallel emission is favored in π-S and forbidden in HB perfect lattices.[24,25] We argue now that in an amorphous film we can have local ordering, with only partial nearest-neighbor filling, which naturally breaks the symmetry. In this case, the exciton can be formed by light capture at a given active site (here understood as a cluster of small conjugated segments), or formed by electron-hole interaction at that site, which would be characterized by that partial symmetry. We simulate this behavior by building small clusters of PV oligomers (from P3V2 to P7V6, up to three oligomers per cluster) organized in partial π-S and HB local arrangements. All clusters were taken from the ideal crystalline packing structures[25]. We simulated the optical properties *in vacuum* (isolated clusters), that is, the calculated transition energies are not mediated by the permittivity of the film and thus we do not expect a quantitative energy spectrum, but a qualitative picture of the optical behavior of a stretched film.

We show in Figure 6 the lowest-energy transitions for four clusters arranged in local π-S symmetry, analysing already the polarization intensity along the perpendicular (y) and parallel (z) directions. As expected, longer chains produce lower-energy optical transitions. In all cases the qualitative picture is in agreement with the results[25,26] for solid-state π-stacking: the first exciton (direct) is polarized along the parallel direction, and we have a higher-energy (charge-transfer) exciton, with non-negligible oscillator strength, polarized along the perpendicular direction. In this case, we can also expect for the aligned π-S bundle in the amorphous region the conversion of polarization, that is, if the incident beam is polarized in the perpendicular direction, we will have absorption, then internal decay followed by emission in the parallel direction.

Concerning HB local arrangement, Figure 7 shows the results for this local arrangement for two clusters. We can observe optical activity in both polarizations, and along the z-direction (direct exciton) the behavior is very close to that seen for the crystal, we have an almost dark excitation at lower energy, but now with non-negligible oscillator strength. More interesting, this excitation for the cluster is of partial charge-transfer character, that is, can absorb also in the perpendicular polarization (y), and since the oscillator strength is larger in the z-component, it will probably decay in parallel polarization.

Summarizing our results for the optical properties of the oligomer clusters we find that always, be in partial π-S or HB packing, we will have i) lower, but not null absorption intensity in

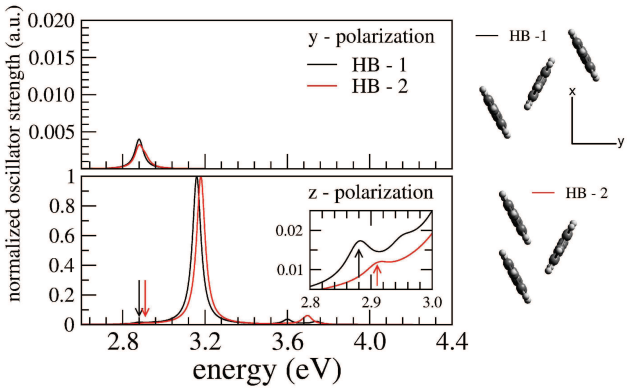

Fig. 7 Electronic absorption spectra calculated for two (P4V3) oligomer clusters in partial HB local arrangements, as sketched on the right. Top, contribution of polarization intensity along the y-axis (perpendicular to the chain backbone), bottom along the z-axis (parallel). The spectra are obtained through a Lorentzian broadening of 25 meV, and further normalized in each calculation by setting to 1.0 the main peak in the chain direction.

the perpendicular direction, and ii) probable conversion in emission to the parallel direction. We stress that this does not require either crystallization of large cells, or stability of one arrangement (π-S) over the other (HB) with time.

5 Conclusions

In this work we carried out both experimental and theoretical investigations on the behavior of polarized emission of stretched PPV films. Experiment showed that for the stretched film optical emission is less intense when the incident light is polarized perpendicular to the stretch direction ***S*** compared to incident light polarized parallel to ***S***. Moreover, we see conversion of polarization, that is light absorbed in the perpendicular polarization is emitted with polarization parallel to the stretch direction.

Our theoretical simulation of amorphous PPV films under stretch showed that overall the polymer chains align to the stretch direction, and that local inter-chain packing, π-S and HB, increases. Both effects can qualitatively explain anisotropic optical behavior. In the first place, the overall alignment to ***S*** will damp absorption from a perpendicular polarized light source as a whole, since the optical activity of a conjugated linear chain is constrained to the parallel polarization. On the other hand, local packing of conjugated segments, from neighbor chains in the amorphous regions, intensifies that same perpendicular polarization absorption by creating local π-stacking or partial herringbone symmetry clusters, that not only can absorb in the perpendicular polarization, but more relevant will emit in the parallel polarization. Our results further indicate that this polarization-conversion property is not exclusively restricted to local (unstable) π-S clustering, since in the amorphous setting it will also be carried by HB clusters.

6 Acknowledgements

The authors are grateful to the Brazilian funding agencies FAPESP, CAPES (Proc. Number: PNPD0052086), CNPq, and the National Institute of Science and Technology on Organic Electronics (INEO/INCT) for financial support and fellowships.

References

1 D. D. C. Bradley, R. H. Friend, H. Lindenberger and S. Roth, *Polymer*, 1986, **27**, 1709 – 1713.
2 D. D. C. Bradley, *J. Phys. D*, 1987, **20**, 1389–1410.
3 T. Granier, E. L. Thomas, D. R. Gagnon, F. E. Karasz and R. W. Lenz, *J. Polym. Sci. Pol. Phys.* , 1986, **24**, 2793–2804.
4 J. Briers, W. Eevers, P. Cos, H. J. Geise, R. Mertens, P. Nagels, X. B. Zhang, G. Van Tendeloo, W. Herrebout and B. Van der Veken, *Polymer*, 1994, **35**, 4569–4572.
5 R. H. Friend, *Pure Appl. Chem.* , 2001, **73**, 425–430.
6 J. C. Scott, in *History of Conductive Polymers*, ed. A. Eftekhari, John Wiley & Sons, Ltd, 2010, pp. 1–17.
7 C. Y. Yang, K. Lee and A. J. Heeger, *J. Mol. Struct.* , 2000, **521**, 315 – 323.
8 D. Sainova, A. Zen, H.-G. Nothofer, U. Asawapirom, U. Scherf, R. Hagen, T. Bieringer, S. Kostromine and D. Neher, *Adv. Func. Mater.* , 2002, **12**, 49–57.
9 C. Soci, D. Comoretto, F. Marabelli and D. Moses, *Phys. Rev. B*, 2007, **75**, 075204.
10 A. Montali, C. Bastiaansen, P. Smith and C. Weder, *Nature (London)*, 1998, **392**, 261 – 264.
11 T. Miteva, A. Meisel, M. Grell, H. G. Nothofer, D. Lupo, A. Yasuda, W. Knoll, L. Kloppenburg, U. H. F. Bunz, U. Scherf and D. Neher, *Synth. Met.* , 2000, **111-112**, 173–176.
12 M. C. Gather and D. D. C. Bradley, *Adv. Func. Mater.* , 2007, **17**, 479–485.
13 L. Biniek, N. Leclerc, T. Heiser, R. Bechara and M. Brinkmann, *Macromol.*, 2013, **46**, 4014–4023.
14 P. D. Townsend, C. M. Pereira, D. D. C. Bradley, M. E. Horton and R. H. Friend, *J. Phys. C*, 1985, **18**, L283–L289.
15 R. Ou, G. Cui, R. A. Gerhardt and R. J. Samuels, *Electrochimica Acta*, 2006, **51**, 1728–1735.
16 M. J. Lee, D. Gupta, N. Zhao, M. Heeney, I. McCulloch and H. Sirringhaus, *Adv. Func. Mater.* , 2011, **21**, 932 – 940.
17 T. M. S. Wilson, D. A. Chinn, D. B. Robinson and F. P. Doty, *Appl. Phys. Lett.* , 2008, **93**, 143304.
18 V. Morandi, M. Galli, F. Marabelli and D. Comoretto, *Phys. Rev. B*, 2009, **79**, 045202.
19 V. Morandi, M. Galli, F. Marabelli and D. Comoretto, *J. Appl. Phys.* , 2010, **107**, 073106.

20 J. Ridley and M. Zerner, *Theor. Chem. Acta*, 1973, **32**, 111–134.

21 A. Marletta, F. A. Castro, C. A. M. Borges, O. N. Oliveira, R. M. Faria and F. E. G. Guimarães, *Macromol.*, 2002, **35**, 9105–9109.

22 A. Marletta, R. H. Miwa, T. Cazati, F. E. G. Guimarães, R. M. Faria and M. Veríssimo-Alves, *Appl. Phys. Lett.* , 2005, **86**, 141907–141907–2.

23 C. A. Olivati, M. Ferreira, T. Cazati, D. T. Balogh, F. E. G. Guimarães, O. N. Oliveira and R. M. Faria, *Chem. Phys. Lett.* , 2003, **381**, 404–409.

24 A. Ruini, M. J. Caldas, G. Bussi and E. Molinari, *Phys. Rev. Lett.* , 2002, **88**, 206403.

25 G. Bussi, A. Ferretti, A. Ruini, M. J. Caldas and E. Molinari, *Adv. Solid State Phys.* , 2003, **43**, 313–326.

26 A. Ruini, A. Ferretti, G. Bussi, E. Molinari and M. J. Caldas, *Semicond. Sci. Technol.* , 2004, **19**, S362–S364.

27 W. Barford, E. R. Bittner and A. Ward, *J. Phys. Chem. A*, 2012, **116**, 10319 – 10327.

28 A. K. Rappé, C. J. Casewit, K. S. Colwell, W. A. Goddard III and W. M. Skiff, *J. Am. Chem. Soc.* , 1992, **114**, 10024–10039.

29 R. Ramos, J. G. Amazonas, M. F. Siqueira, M. Pinheiro, R. Lelis-Sousa, M. Alves-Santos and M. J. Caldas, *to be published*, 2015.

30 A. Tkatchenko and M. Scheffler, *Phys. Rev. Lett.* , 2009, **102**, 073005.

31 V. Blum, R. Gehrke, F. Hanke, P. Havu, V. Havu, X. Ren, K. Reuter and M. Scheffler, *Comput. Phys. Commun.* , 2009, **180**, 2175 – 2196.

32 F. L. Hirshfeld, *Theor. Chem. Acta*, 1977, **44**, 129–138.

33 C. Y. Yang, F. Hide, M. A. Diaz-Garcia, A. J. Heeger and Y. Cao, *Polymer*, 1998, **39**, 2299–2304.

34 A. M. Machado, M. Munaro, T. D. Martins, L. Y. A. Davila, R. Giro, M. J. Caldas, T. D. Z. Atvars and L. C. Akcelrud, *Macromol.*, 2006, **39**, 3398–3407.

35 R. Giro, L. Y. A. Davila, A. M. Machado, M. J. Caldas and L. Akcelrud, *Int. J. Quantum Chem.*, 2010, **110**, 885–892.

36 M. De Corato, C. Cocchi, D. Prezzi, M. J. Caldas, E. Molinari and A. Ruini, *J. Phys. Chem. C*, 2014, **118**, 23219–23225.

37 *Cerius*^{2}*, version 4.6 – Accelrys Inc.*, 2001.